Degradation and mechanism of microcystin-LR by $PbCrO_4$ nanorods driven by visible light

Liu, Guoshuai; Zhang, Guoqiang; Zhang, Shuo; Xu, Yangsen; Yang, Xun; Zhang, Xuedong

DOI
10.1016/j.chemosphere.2019.124739

Publication date
2020

Document Version
Final published version

Published in
Chemosphere

Chemosphere 239 (2020) 124739

Contents lists available at ScienceDirect

Chemosphere

journal homepage: www.elsevier.com/locate/chemosphere

Degradation and mechanism of microcystin-LR by $PbCrO_4$ nanorods driven by visible light

Guoshuai Liu [a, c], Guoqiang Zhang [b, d, *], Shuo Zhang [c], Yangsen Xu [d], Xun Yang [e], Xuedong Zhang [c]

[a] State Key Laboratory of Urban Water Resource and Environment, School of Environment, Harbin Institute of Technology, Harbin, 150090, PR China
[b] College of Chemistry and Environmental Engineering, Shenzhen University, Shenzhen, 518060, PR China
[c] Department of Water Management, Section Sanitary Engineering, Delft University of Technology, PO Box 5048, 2600, GA, Delft, Netherlands
[d] International Collaborative Laboratory of 2D Materials for Optoelectronics Science and Technology of Ministry of Education, Institute of Microscale Optoelectronics, Shenzhen University, Shenzhen, 518060, China
[e] School of Physics, Zhengzhou University, Zhengzhou, 450052, China

HIGHLIGHTS

- Efficient MC-LR degradation by PbCrO4 photocatalyst.
- PbCrO4 energy band structure and density of state was under detailed investigation.
- Degradation mechanism was studied in principle and experimental method.

GRAPHICAL ABSTRACT

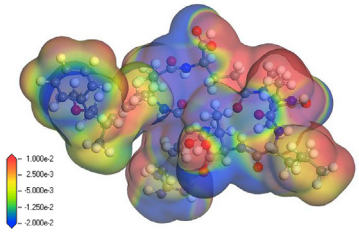

Effective MC-LR photocatalytic removal through hydroxyl radical attack by $PbCrO_4$ photocatalyst.

ARTICLE INFO

Article history:
Received 2 July 2019
Received in revised form
22 August 2019
Accepted 31 August 2019
Available online 10 September 2019

Handling Editor: Yongmei Li

Keywords:
$PbCrO_4$ single crystal
Photocatalysis
MC-LR
Degradation and mechanism
•OH radicals

ABSTRACT

This work focuses on the photocatalytic removal of recalcitrant organic pollutants in water treatment. Based on facile precipitation reaction, we fabricated a photocatalyst ($PbCrO_4$) in single crystals that present evident response to visible light and employed the catalyst in the photocatalytic decomposition of microcystin-LR (MC-LR). In the degradation test using the nanorods with prepared $PbCrO_4$ photocatalyst, a 100% removal efficiency (27 min reaction) and a kinetics constant of 0.1356 min^{-1} were achieved. Such a high performance of $PbCrO_4$ in photocatalytic conversion of MC-LR was ascribed to its high carrier separation efficiency, positive valence band (VB) position, and good delocalization of VB and conduction band (CB). The test of electron spin-resonance resonance (ESR) demonstrated that excessive free •OH radicals were produced during the $PbCrO_4$ photocatalysis of MC-LR. The density functional theory (DFT) and LC/MS/MS technology were employed to ascertain the intermediates during the MC-LR photocatalytic degradation. The major intermediates were resulted from the attack of hydroxyl radicals to the ADDA side chains of MC-LR structure. This study provides a proof-of-concept strategy to develop effective photocatalysts to efficiently produce •OH radicals for the visible-light induced photocatalytic degradation of MC-LR in water.

* Corresponding author. College of Chemistry and Environmental Engineering, Shenzhen University, Shenzhen, 518060, PR China.
E-mail address: zhangguoqiang@szu.edu.cn (G. Zhang).

https://doi.org/10.1016/j.chemosphere.2019.124739
0045-6535/

1. Introduction

Accompanying with the rapid development of human societies and industry in the past decades, eutrophication of water environment due to overgrowing cyanobacteria (blue-green algae) frequently occurs and becomes increasingly severe. Cyanotoxins as a typical metabolite produced by cyanobacteria greatly threaten human health. Microcystins are a group of cyclic seven peptide substances containing ADDA side chains, which are the strongest promoters of liver tumor (Choi et al., 2007; Graham et al., 2010; Paerl et al., 2011; Gupta et al., 2013). Amongst them, Microcystin-LR (MC-LR) is one of the most toxic microcystins produced by cyanobacteria, and the polycyclic structure of MC-LR makes it stable in a wide range of pH and temperatures (Gupta et al., 2013). Many treatment techniques have been studied to effectively remove MC-LR, such as coagulation, adsorption, biological and membrane technologies (Lawton and Robertson, 1999; Lee and Walker, 2006; Wang et al., 2017; Zhang et al., 2017), but with limited success. Besides, the techniques may even cause rupture of algal cells and release algal toxins into water bodies, potentially leading to a risk of secondary pollution. Therefore, further effective and efficient advanced treatment to remove MC-LR is urgently needed. The oxidative •OH produced via photocatalytic water oxidation process has been introduced to water treatment extensively because the radicals can react with target organics via H-abstraction or addition reactions to unsaturated bonds (Han et al., 2009, 2011; Silva and Faria, 2010). In the framework of MC-LR, its inbuilt structure of aromatic ring, diene bond, methoxy group of the ADDA chains, and the double bond of MDHA residue, can be attacked by •OH radicals in principle and lead to the degradation of MC-LR (Gao et al., 2009; Han et al., 2009, 2011; Silva and Faria, 2010; Shao et al., 2017).

TiO_2-based semiconductors have been extensively investigated in the removal of MC-LR using UV-light driven photocatalytic processes (Hoffmann et al., 1995; Antoniou et al., 2009; Pelaez et al., 2010; Morales-Torres et al., 2012). However, there are still some challenges in the photocatalysis of MC-LR mediated by TiO_2-based semiconductors due to the following aspects. First, TiO_2 is a typical UV light photocatalyst with a wide band gap ($E_g \approx 3.2$ eV), whereas the UV light just accounts for 4% of the region of the solar light spectrum (Choi et al., 2006; Li et al., 2018). Second, carrier separation is a bottleneck that limits its photocatalytic efficiency (Liu et al., 2017b). Lastly, the transformation mechanism of MC-LR induced by •OH under visible-light is still unclear and needs further investigation. With this context, evidently there is a need to develop an efficient, active and visible−light induced photocatalyst for MC-LR removal and to further clarify the transformation mechanism in the degradation of MC-LR in detail.

$PbCrO_4$ (the mineral crocoite) crystallizes at ambient pressure in the monoclinic monazite structure (space group P21/n, Z = 4). The structural arrangement of monazite is based on the nine-fold coordination of the Pb and the fourfold coordination of Cr, and with good visible-light absorption (Liang and Li, 2004). Monazite-type oxides form an extended family of compounds. Because of its excellent photostability and relatively easy accessibility, several applications of these materials are already reported or under development. These applications include photoconductive dielectric materials (Abdul-Gader and Wishah, 1997), humidity sensing resistors (Cheng et al., 2007), yellow pigments (Amat et al., 2016), effective solid lubricants (Wang et al., 2007), and visible light-driven photocatalyst for splitting water molecules, which is associated with a hydroxyl radical process (Zhang et al., 2018). Although $PbCrO_4$ photocatalyst was evidently proved to be capable of promoting production of hydroxyl radical, the photocatalytic use of $PbCrO_4$ for decomposing organic compounds was overlooked.

In this present study, we fabricated stable and highly active visible-light driven photocatalyst $PbCrO_4$ by a facile precipitation reaction. First, the crystal structure and microcosmic morphology of prepared $PbCrO_4$ photocatalyst were measured using X-ray diffraction (XRD) and transmission electron microscopy (TEM). Second, the energy band and electron configuration of the crystals were theoretically determined by the calculation based on density functional theory (DFT) and ultraviolet photoelectron spectroscopy (UPS). Third, the photocatalytic degradation of MC-LR was examined in detail in the aspects of removal performance and kinetics. Last, the degradation and transformation mechanisms of MC-LR were elucidated using experimental results and the DFT calculation.

2. Materials and methods

2.1. $PbCrO_4$ nanorods preparation

All the chemicals used for the preparation of $PbCrO_4$ nanorod were of analytical grade. $Pb(NO_3)_2$ (Aladdin Reagent Company), $Na_2CrO_4 \cdot 4H_2O$ (Aladdin Reagent Company), and MC-LR were purchased from Beijing Puhuashi Technology Company, China and the commercial $PbCrO_4$ was purchased from Sinopharm Co. Ltd. During the typical $PbCrO_4$ nanorod synthesis, 50 mL of a 0.4 M $Pb(NO_3)_2$ solution and 50 mL of a 0.4 M Na_2CrO_4 solution were mixed and stirred for 120 min at 20 °C. The harvested yellow deposits were rinsed with DI-water to remove the residual impurities and then were placed into a vacuum drying chamber at 60 °C until for the further use and characterization.

2.2. Characterizations

The X-ray diffraction (XRD) was performed using X-ray diffractometer (Bruke D8 Adv.; Germany). The morphology and crystalline structure of prepared samples was recorded on transmission electron microscopy (TEM) and high-resolution TEM (HRTEM) on F-30ST (Tecnai, FEI, U.S.) and FESEM-4800 field emission scanning electron microscope (SEM, Hitachi, Japan). The optical property was acquired using a UV−Vis spectrophotometer (Type-UV2550, Shimadzu, Japan). UPS spectra were measured using He I excitation (21.2 eV) and recorded with a pass energy of 5 eV in the ultra-high vacuum (UHV) chamber of the XPS instrument (PHI 5600-CI, Physical Electronics, U.S.). UPS binding energies were referenced to the Fermi edge of Au, which was sputtered onto the sample in the UPS chamber. Zeta potential of the $PbCrO_4$ samples was recorded by a zeta potential analyzer (Nano-Z, Malvern Corp., U.S.) at stepwise change of pH of samples adjusted by HCl (1.0 M) and NaOH (1.0 M). In the analysis of zeta potential, sample concentration 0.001 w/v %, DI water was used as solvent, and equilibrium time 30 min. The ESR signals of the radicals that were spin-trapped by 5,5-dimethyl-1-pyrroline-N-oxide (DMPO) were examined with a Bruker A300 spectrometer. The irradiation source was a 300 W xenon lamp with a UVCUT-420 nm filter. The settings for the ESR spectrometer were center field of 3510.00 G, microwave frequency of 9.79 GHz, and power of 5.05 mW (Liu et al., 2017a; 2017b).

2.3. DFT calculation

In order to understand the electronic configuration of $PbCrO_4$, the DFT calculation was implemented using the DMol^3 program. In detail, the exchange correlation effects were depicted by the generalized gradient approximation (GGA) developed by Perdew, Burke, and Ernzerhof (PBE) (Ji et al., 2016; Liu et al., 2019). The molecular orbitals were expanded into a double-numerical basis with polarization functions (DNP). The criterion of self-consistent field convergence was set to an energy change of 10^{-6} hartree. The optimal criteria of geometry convergence in terms of the

energy, force and displacement convergence were 1×10^{-5} Hartree, 2×10^{-3} Hartree/Å and 5×10^{-3} Å, respectively. The Brillouin zone integrations were conducted by a $4 \times 3 \times 4$ Monkhorst-pack k-point grid.

2.4. 2.4 Photocatalytic experiments with MC-LR

The visible-light driven photocatalytic conversion of MC-LR by $PbCrO_4$ was carried out using a Xenon lamp (300 W; CELHXF300, Ceaulight Co. Ltd., China) equipped with a 420 nm cut filter and an average light intensity of 100 mW cm^{-2} in a stirred batch-fed beaker at the ambient temperature (25 ± 1 °C). In a typical test of photocatalytic degradation of organic matter, the photocatalyst, $PbCrO_4$ (0.5 g L^{-1}, pH = 7), was homogeneously dispersed into 60 mL of an MC-LR solution (1000 ± 10 μg L^{-1}, pH 6.8 ± 0.4) by stirring for 10 min. Prior to the tests, an adsorption-desorption equilibrium of the solution was reached. Then, the mixed solution was exposed to the irradiation of visible light, taking the liquid samples at a given interval for analysis after centrifugation at 8000 rpm and filtration using 0.2 μm filters of cellulose acetate membrane. The degradation rate and reaction intermediates were evaluated using a high-performance liquid chromatography (HPLC, Agilent Series 1100). For the HPLC, the injection volume to a Discovery C-18 column (Supelco) at 40 °C was 50 μL. The mobile phase in isocratic mode with a flow rate of 1 mL/min was a mixture of 0.05% trifluoroacetic acid (TFA) in water and 0.05% TFA in acetonitrile at a ratio of 60:40. MC-LR was eluted at 5.4 min and measured with a photodiode array detector at 238 nm. For the identification of the intermediates with LC/MS, a gradient method was used with a mixture of 0.1% formic acid in acetonitrile and 0.1% formic acid in water. A Thermo Finnigan LCQ Deca ion trap mass spectrometer was utilized for the determination of the possible structures of the reaction byproducts (MS/MS analysis) (Choi et al., 2007; Liu et al., 2003; Yanfen et al., 2011; Chen et al., 2012).

3. Results

3.1. Microcosmic structure and morphology

The ball-stick crystal model of $PbCrO_4$ is illustrated in Fig. S1A, where the $PbCrO_4$ crystal was composed of the corner-connected PbO_9 twisted polyhedron and CrO_4 tetrahedron. The XRD of the prepared $PbCrO_4$ (Fig. S1B) demonstrates the monoclinic structure with cell parameters of $PbCrO_4$ (a = 7.12 Å, b = 7.44 Å, c = 6.8 Å; α = 90.0°, β = 102.4°, γ = 90.0°). All the diffraction peaks at 17.87°, 20.31°, 25.58°, 27.17°, 29.46°, 35.18°, 40.00°, 43.25°, 45.84° and 49.30°, can be indexed to (011), (101), (200), (120), (012), (−212), (−103), (212), (−132) and (−322) facets of $PbCrO_4$ (JCPDS No. 08−0209), which indicates the as-synthesized $PbCrO_4$ photocatalyst with high crystallinity and purity (Zhang et al., 2017; Mei et al., 2007). The microcosmic morphologies of prepared $PbCrO_4$ were investigated by SEM and TEM, and the corresponding images are as shown in Figs. S1C, D and E. As it shows, the $PbCrO_4$ is well defined nanorods with a range of diameters from 50 to 120 nm, and the length of 4 μm. The aspect ratios of $PbCrO_4$ nanorods are up to 80, and each nanorod is straight and presents a uniform diameter along its entire length. The analysis of energy dispersive X-ray analysis (EDX) (Fig. S2) shows the element molar ratio of Pb, Cr and O is close to 1:1:4, indicating that the well-defined stoichiometric $PbCrO_4$ crystal was prepared. Fig. S1F shows the HRTEM image of an individual nanorod, which demonstrated a single-crystalline feature of $PbCrO_4$ with a periodic d-spacing of 5.10 Å along the longitudinal direction of the nanorod, which was indexed to the (110) plane of monoclinic $PbCrO_4$ (Liang and Li, 2004). This indicates that the prepared $PbCrO_4$ photocatalyst in this present work was single crystal nanorod, and the growth direction was c axis.

Fig. S3 shows the XPS spectra of $PbCrO_4$, and the binding energies at 142.9, 138.2, 588.1 and 578.9 eV are assigned to Pb $4f_{5/2}$, Pb $4f_{7/2}$, Cr $2p_{1/2}$ and Cr $2p_{3/2}$, respectively (Zhang et al., 2017). The binding energy of O 1s located in 529.9 eV is ascribed to the lattice oxygen, and the peak at 531.9 eV is ascribed to the surface O or the surface OH groups (Zhang et al., 2017). The XPS spectra of $PbCrO_4$ nanorods indicate the prepared photocatalyst was with no impurity in other metallic valences.

3.2. 3.2 Photocatalytic decomposition of MC-LR

The photocatalytic performance was recorded during the degradation of MC-LR under visible light, and the commercial $PbCrO_4$ was used for comparison. As shown in Fig. 1A, under visible light irradiation ($\lambda \geq 420$ nm), the MC-LR concentration almost remained no changes, which excludes the possibilities of self-degradation caused by visible-light induced photocatalysis without addition of the photocatalyst. Besides, after 30 min of dark equilibration, the percentage of MC-LR adsorbed on the surface of $PbCrO_4$ nanorods was approximately 10%, which indicates that the high conversion of MC-LR was not mainly resulted from adsorption. In the presence of commercial $PbCrO_4$, the MC-LR removal efficiency is up to 70% in 27 min under visible light. The harvested $PbCrO_4$ single crystal nanorods displayed much higher degradation efficiency of MC-LR than the commercial $PbCrO_4$ sample. MC-LR was almost completely removed in 27 min by the as-prepared $PbCrO_4$ nanorods. The linear dependence of $\ln(C_t/C_0)$ as a function versus time further verifies the pseudo-first-order kinetics in the removal of MC-LR under the visible-light driven photocatalysis with $PbCrO_4$. As revealed by Fig. S4, the degradation rate constants of MC-LR in the tests with additions of $PbCrO_4$ nanorods and commercial $PbCrO_4$ were 0.1356 and 0.0471 min^{-1} (Table S1), respectively. The degradation rate of the MC-LR with single crystal nanorods of as-prepared $PbCrO_4$ is 2.88 times higher than that of commercial $PbCrO_4$. This might be attributed to the differences in the structure of the crystals. The as-prepared $PbCrO_4$ was well defined nanorods of single crystals, and however the commercial $PbCrO_4$ was poly-crystalline. The photocatalytic activity highly depends on the catalyst structure, which is also tightly associated with the efficiency in carrier separation. The impact of photocatalyst dosage on MC-LR degradation performance was also investigated, and the corresponding results are shown in Fig. 1B. When the dosage of $PbCrO_4$ nanorods increased from 0.2 g L^{-1} to 0.5 g L^{-1}, the removal efficiency of MC-LR also subsequently increased from 81% to 100%, during 27 min, with a kinetics constant increasing from 0.0649 to 0.1356 min^{-1} (Fig. S5 and Table S2). With the further increase of the dosage to 1.0 g L^{-1}, the degradation performance in term of degradation rate was not changed substantially than that of 0.5 g L^{-1}. The results indicate the photocatalytic decomposition of MC-LR was dependent on the dosage of the photocatalyst, but there was an upper limit because of the utmost light utilization efficiency. pH is a crucial parameter in practical water environment. As illustrated in Fig. 1C, the degradation efficiency of MC-LR decreased substantially when the initial solution pH increased from 2.0 to 11.0, with a decrease in kinetic constants from 0.2121 to 0.0562 min^{-1} almost by 74% (Fig. S6 and Table S3). The p*K*a of the free carboxyl group at the D-Glu side is 2.10 (Mei et al., 2007), and therefore in the pH range (2.0−11.0) in the present study, the carboxyl group was mainly deprotonated and negatively charged. The surface potential pH_{PZC} of $PbCrO_4$ was 3.8 (Fig. S7), i.e., the surface of $PbCrO_4$ was positively charged, when the pH decreased to <3.8, otherwise vice versa. Therefore, under the condition of pH < 3.8, the negatively charged Glu-MDHA side of MC-LR and the positively charged $PbCrO_4$ surface presented a

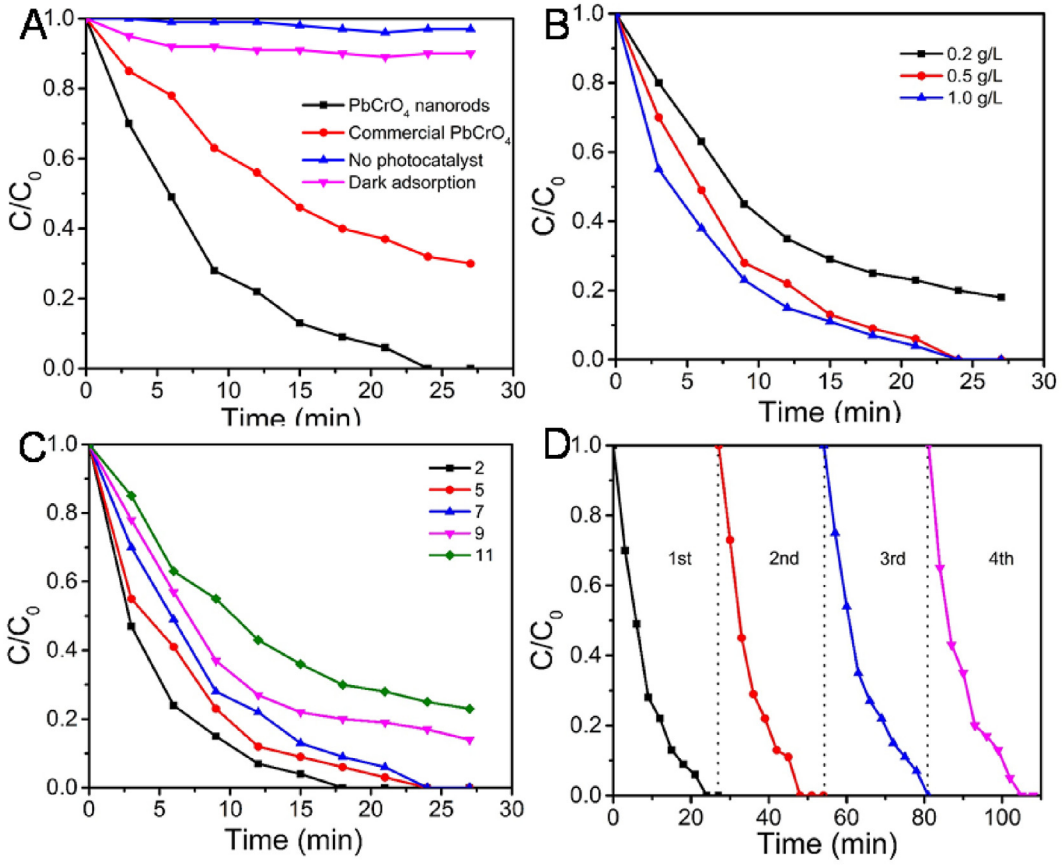

Fig. 1. The photocatalytic degradation of MC-LR using $PbCrO_4$ nanorods and commercial $PbCrO_4$ (A). The effects of variations of photocatalyst dosage (B) and pH (C) on the performance of the degradation of MC-LR. D is the stability test of recycled photocatalyst.

strong electrostatic attraction force. $PbCrO_4$ displayed good adsorption ability to MC-LR under acidic aquatic conditions, thus leading to a high removal efficiency of MC-LR. The stability of photocatalyst is of great importance from the viewpoints of cost-effectiveness in practical applications. Thus, the cyclic tests over $PbCrO_4$ nanorods were documented to assess their stability, as demonstrated in Fig. 1D, and the $PbCrO_4$ showed almost no inactivation after being recycled 4 times. Besides, we performed a very broad pH range from 2 to 11 for degrading MC-LR, and the ICP test also was implemented to clarify that the residue of lead and chromate ions in the reaction solution at different pH (Fig. 1C). The ICP tests indicated that the concentrations of Pb and Cr gradually increased as the pH decreased (Data not show). The contents of the residual lead and chromate ions were lower in the pH range of 5—11 than that at pH of 2. These results show that this visible-light induced active photocatalyst $PbCrO_4$ released concentrations of negligible lead and chromate ions under pH conditions from 11 to 5. Whereas the contents of the residual lead and chromate ions were relatively high under pH of 2, this issue may be mitigated by the construction of heterogeneous photocatalyst system or element doping, and will be considered in the future study. Furthermore, in order to decipher which oxidative species were dominant in the process of MC-LR removal, the corresponding tests of scavenging activity were implemented and the results were summarized in Table S4. It is well recognized that benzoquinone (BQ) is an effective $\cdot O_2^-$ trapper, and tert-butanol (TBA) is a typical •OH radicals' scavenger (Liu et al., 2017b). As illustrated in Table S4, BQ exhibited a slight impact on MC-LR degradation, whereas the addition of TBA led to substantial suppression on MC-LR removal. The phenomena indicate that the involved reactive species during the MC-LR degradation was mainly •OH radicals. According to the Nernst equation, with the increase of pH, the oxidation power of •OH decreases (Rao and Hayon, 1974; Kapałka et al., 2009; Liu et al., 2017a), which might be another reason why the performance of MC-LR degradation decreased under alkaline niches.

3.3. Electronic structure of $PbCrO_4$

Despite of the surface properties, photocatalytic activity reflects its intrinsic photo-generated electron/hole pairs, which substantially depends on its electron configuration (Tang et al., 2004). Diffuse reflectance spectroscopy (DRS) is a common technology to understand the electronic states of photocatalysts. The dark yellow powders (inset of Fig. S8A) had a strong absorption band at the region of visible light, which indicates that the $PbCrO_4$ nanorods could harvest visible light up to 550 nm. The energy band gap (E_g) of $PbCrO_4$ nanorods was obtained using a classical Tauc approach.

According to the following equation (Pan and Zhu, 2010, 2011; Zhou et al., 2010),

$$\alpha h\nu = A(h\nu - E_g)^{n/2} \quad (1)$$

where α is the optical absorption coefficient, A is the proportionality constant, and $h\nu$ is the photonic energy. n is correlated to the type of indirect/direct semiconductor. Considering the indirect transition property of $PbCrO_4$, which is depicted in the following DFT calculation of band structure, substituting $n = 4$ in Eq. (1) gives the E_g of 2.11 eV (Fig. S8B).

As shown in the test of radical scavenging activity, the photocatalytic degradation of MC-LR by $PbCrO_4$ depended on the hydroxyl radicals, which was associated with the oxidation power of photo-generated hole that was generated on the position of valence band. To thermodynamically clarify the relationship of the valence band energy (EVB) of $PbCrO_4$ versus standard hydrogen electrode (SHE), tests using ultraviolet photoelectron spectroscopy (UPS) were carried out. As shown in Fig. 2, the measured EVB was 2.45 V versus SHE, and a conduction band energy (ECB) was 0.34 V versus SHE. The EVB value is 0.56 V higher than the potentials of OH/•OH (1.89 V, alkaline solution) (Koppenol and Liebman, 1984; Schwarz and Dodson, 1984; Liu et al., 2016), which demonstrated the generation of •OH and a thermodynamic feasibility over the $PbCrO_4$ nanorods under the irradiation of visible light.

To in-depth understand the $PbCrO_4$ intrinsic electronic configuration, the calculations using density functional theory (DFT) were implemented. The band structure diagram is presented in Fig. 3A and density of states (DOS) in Fig. 3B. The conduction band maximum (CBM) and valence band minimum (VBM) are located at different k-point, which implied a typical indirect semiconductor property (Dianat et al., 2013; Wang et al., 2015). For the photocatalysts of indirect transition semiconductors, the emission of excited electrons is coordinated by phonon generation. In this context, the activity and lifetime of the catalyst can be maintained, and the photo-generated electron/hole pairs can effectively participate in the redox reaction. Besides, the band gap was calculated to be 1.51 eV between VBM and CBM (Fig. 3A), which is 0.60 eV smaller than that of the experimental value (2.11 eV). The difference is caused by the well-known effect of generalized gradient approximation (GGA) (Kohn et al., 1996; Gritsenko et al., 2000). As illustrated in the DOS curves (Fig. 3B), the bottom of CB mainly originated from Cr 3 d orbital hybrid with O 2p. The deep VB was mainly composed by the electrons at Cr 3 d orbital and O 2p orbital and the valence band near the fermi level originated from the O 2p orbital. The DOS curve implies that the intrinsic absorption edge of $PbCrO_4$ was determined by the electrons that were excited from the 2p orbital of O to the 3 d orbit of Cr. Then consequently the excitation led to photocatalytic activity of $PbCrO_4$ under the irradiation of visible light. Furthermore, both the VBM and the CBM showed evident delocalization, which is beneficial for the drift and separation of photo-generated carriers and is therefore conducive to enhancing the photocatalytic performance (Geuenich et al., 2005).

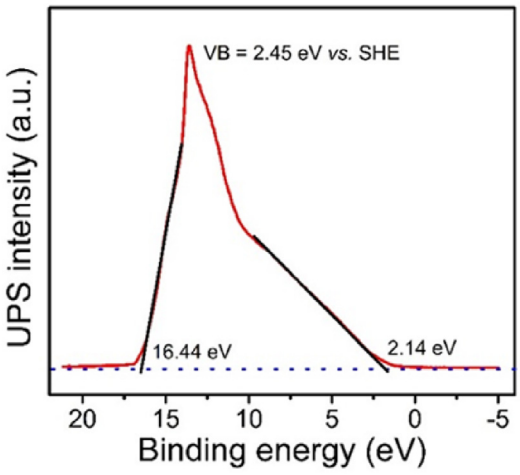

Fig. 2. The UPS spectrum of $PbCrO_4$ nanorods.

3.4. Photoelectrochemical and ESR analysis

The transient photocurrent responses of a photocatalyst are closely related to the recombination efficiency of photo-generated carriers (Kohtani et al., 2005; Zhang et al., 2008; Kandiel et al., 2010). Fig. 4A shows that the photocurrent with good reproducibility, stability and reversibility for $PbCrO_4$ could be attained during five on-off cycles of measurements. Specifically, the photocurrent of as-prepared $PbCrO_4$ nanorods was approximately 9 times of that of commercial $PbCrO_4$, implying the prepared $PbCrO_4$ nanorods seemingly presented higher carrier separation efficiency than the commercial $PbCrO_4$. Based on the results and discussion, we hypothesized that the pre-dominant reactive species during the MC-LR degradation was •OH radical. To further validate whether the •OH formation was direct or not, the ESR test was carried out. Under visible light irradiation (50 W, 30 min), the ESR signals of characteristic •OH-DMPO adduct were detected for $PbCrO_4$ nanorods and commercial $PbCrO_4$ (Fig. 4B), which demonstrated by quartet lines with peak strength of 1:2:2:1 and hyperfine coupling constants of $\alpha_N = 1.49$ mT and $\alpha_H = 1.49$ mT (g-factor of 2.0055) (Turchi and Ollis, 1990; Gao et al., 2002; You et al., 2016). Besides, the ESR signals of oxidized DMPO radicals (rectangular labeled) featured by a three-line spectrum accompanied with •OH-DMPO were also observed, which is in consistent with the previous report

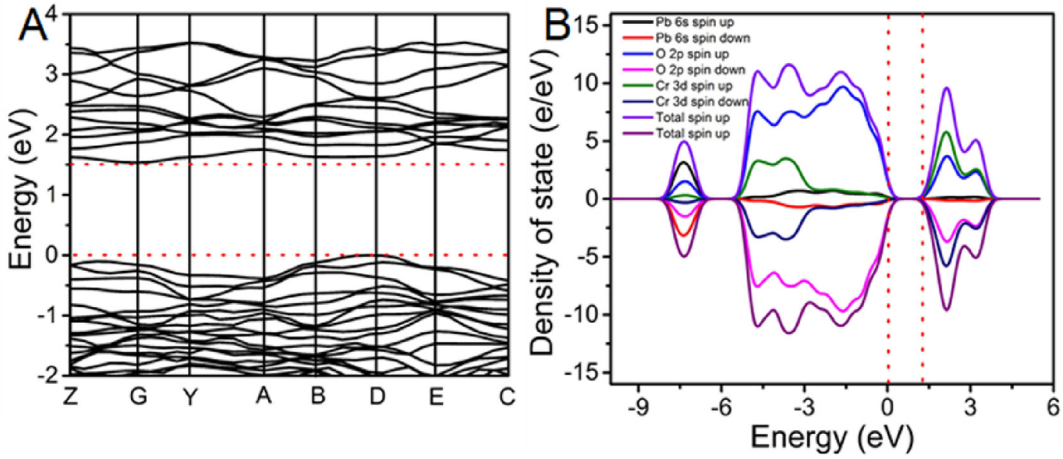

Fig. 3. The band structure (A) and DOS (B) of $PbCrO_4$.

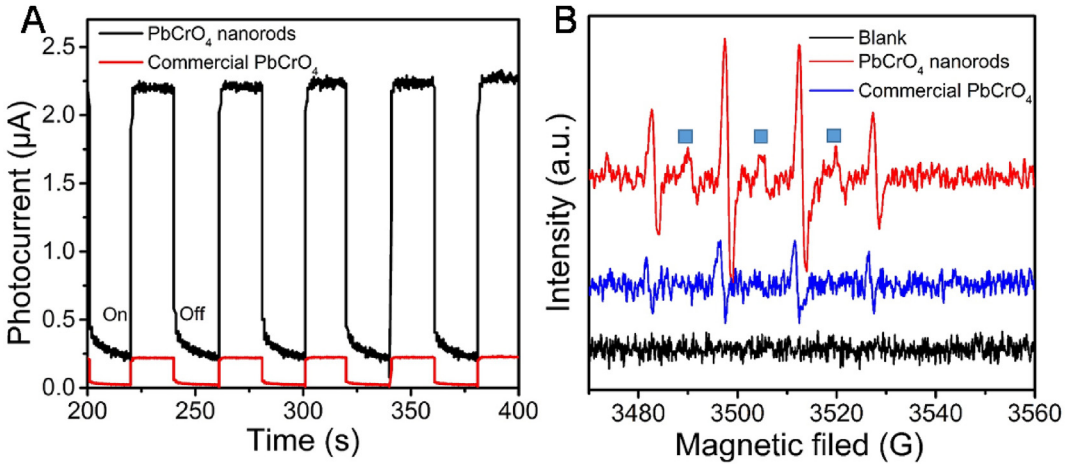

Fig. 4. (A) Time course of photocurrent based on five on-off cycles, and (B) ESR spectra of the test groups of $PbCrO_4$ nanorods and commercial $PbCrO_4$ and the blank group without photocatalyst.

(Feng et al., 2016). Notably, the peak intensity of •OH-DMPO signal for synthesized $PbCrO_4$ nanorods was about 3 times of that for commercial $PbCrO_4$, which explains the enhanced photocatalytic degradation activity of MC-LR with addition of $PbCrO_4$ nanorods under visible light. The results clearly demonstrate that the prepared single crystal $PbCrO_4$ photocatalyst under visible light could effectively promote the formation of hydroxyl radicals which were responsible for the efficient degradation of MC-LR.

3.5. Mechanism of MC-LR photodegradation

Fig. 5A shows the structure scheme of MC-LR molecule, indicating that MC-LR consists of the ADDA, D-Glu, Mdha, D-Ala, L-Leu, D-MeAsp and L-Arg groups. Hydroxyl radical has high electronegativity or electrophilic property, which is prone to attack the structure with high electron cloud density (Buxton et al., 1988). The electron density of MC-LR was calculated using DFT method. Fig. 5B indicates the aromatic ring, conjugated carbon double bonds, and the methoxy group of ADDA presented high electron density. Besides the positions in ADDA, the —NH— related functional groups in D-Glu, Mdha, D-Ala, D-MeAsp and L-Arg side chains also showed high electron density. However, hydroxyl radicals cannot easily attack the positions, because of a high steric hindrance and no unsaturated bonds. Thus, the degradation pathway of MC-LR by photocatalysis involves hydroxyl radical which mainly attacks the aromatic ring, conjugated carbon double bonds and the methoxy group of ADDA. To structurally characterize the degradation products and understand the conversion mechanism of MC-LR by $PbCrO_4$ during the visible-light driven photocatalysis, the reaction broth of MC-LR was analyzed with LC-MS/MS to separate and characterize the principal end-products, and the mass spectra were shown in Figs. S9—S12. MC-LR ($C_{49}H_{74}N_{10}O_{12}$, $m/z = 996$) was converted to one OH-adduct products on aromatic ring and conjugated carbon double bonds ($C_{49}H_{74}N_{10}O_{13}$, $m/z = 1011$), two OH-adduct products ($C_{49}H_{74}N_{10}O_{14}$, $m/z = 1027$) and two OH-adduct products on conjugated carbon double bonds ($C_{49}H_{76}N_{10}O_{14}$, $m/z = 1029$). The dominant degradation intermediates are consistent with the Antoniou's research (Antoniou et al., 2008, 2009) and the DFT prediction.

4. Conclusions

To sum up, the nanorods of $PbCrO_4$ single crystal were successfully developed by a facile precipitation reaction. The prepared $PbCrO_4$ nanorods presented good adsorption ability of visible light, a high separation efficiency of carriers, and a positive valence band position, and thus led to a high efficiency in degradation of MC-LR efficiently. Furthermore, the mechanism of degradation was deciphered using the DFT calculation and experimental methods, indicating that the photocatalytic technology associated with hydroxyl radical is an effective method to remove MC-LR. Overall, this study provides a proof-of-concept demonstration that the $PbCrO_4$ photocatalyst with single crystal is a promising material for the detoxification of cyanotoxin contaminated surface water as drinking water source under visible light irradiation.

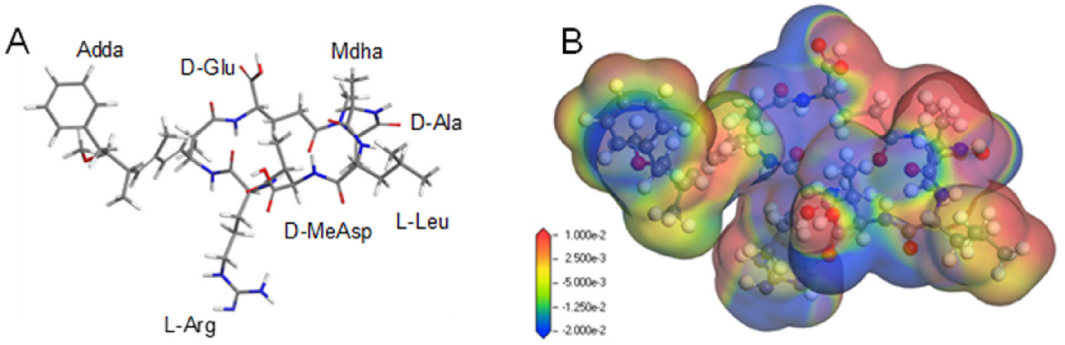

Fig. 5. The molecule structure (A) and electron density (B) of MC-LR.

Acknowledgements

This work was jointly supported by the Science and Technology Project of the Research Foundation of China Postdoctoral Science (2018M630982) and the Natural Science Foundation of China (21401190).

Appendix A. Supplementary data

Supplementary data to this article can be found online at https://doi.org/10.1016/j.chemosphere.2019.124739.

References

Abdul-Gader, M., Wishah, K., 1997. DC I–V characteristics and steady-state photoconductivity of Au/Pb_2CrO_5/SnO_2 sandwich-structure films under illumination in the visible region. J. Mater. Sci. 32, 1269–1275.

Amat, A., Miliani, C., Fantacci, S., 2016. Structural and electronic properties of the $PbCrO_4$ chrome yellow pigment and of its light sensitive sulfate-substituted compounds. RSC Adv. 6, 36336–36344.

Antoniou, M.G., Nicolaou, P.A., Shoemaker, J.A., Armah, A., Dionysiou, D.D., 2009. Impact of the morphological properties of thin TiO_2 photocatalytic films on the detoxification of water contaminated with the cyanotoxin, microcystin-LR. Appl. Catal. B Environ. 91, 165–173.

Antoniou, M.G., Shoemaker, J.A., Cruz, A.A.d.l., Dionysiou, D.D., 2008. Unveiling new degradation intermediates/pathways from the photocatalytic degradation of microcystin-LR. Environ. Sci. Technol. 42, 8877–8883.

Buxton, G.V., Greenstock, C.L., Helman, W.P., Ross, A.B., 1988. Critical review of rate constants for reactions of hydrated electrons, hydrogen atoms and hydroxyl radicals (·OH/·O^- in aqueous solution). J. Phys. Chem. Ref. Data 17, 513–886.

Chen, P., Zhu, L., Fang, S., Wang, C., Shan, G., 2012. Photocatalytic degradation efficiency and mechanism of microcystin-RR by mesoporous Bi_2WO_6 under near ultraviolet light. Environ. Sci. Technol. 46, 2345–2351.

Cheng, B., Guo, H., Yu, J., Zhao, X., 2007. Facile preparation, characterization and optical properties of rectangular $PbCrO_4$ single-crystal nanorods. J. Alloy. Comp. 431, L4–L7.

Choi, H., Antoniou, M.G., Pelaez, M., De la Cruz, A.A., Shoemaker, J.A., Dionysiou, D.D., 2007. Mesoporous nitrogen-doped TiO_2 for the photocatalytic destruction of the cyanobacterial toxin microcystin-LR under visible light irradiation. Environ. Sci. Technol. 41, 7530–7535.

Choi, H., Sofranko, A.C., Dionysiou, D.D., 2006. Nanocrystalline TiO_2 photocatalytic membranes with a hierarchical mesoporous multilayer structure: synthesis, characterization, and multifunction. Adv. Funct. Mater. 16, 1067–1074.

Dianat, A., Seriani, N., Bobeth, M., Cuniberti, G., 2013. Effects of Al-doping on the properties of Li–Mn–Ni–O cathode materials for Li-ion batteries: an ab initio study. J. Mater. Chem. 1, 9273–9280.

Feng, G., Cheng, P., Yan, W., Boronat, M., Li, X., Su, J.-H., Wang, J., Li, Y., Corma, A., Xu, R., 2016. Accelerated crystallization of zeolites via hydroxyl free radicals. Science 351, 1188–1191.

Gao, B., Chen, G.Z., Puma, G.L., 2009. Carbon nanotubes/titanium dioxide (CNTs/TiO_2) nanocomposites prepared by conventional and novel surfactant wrapping sol–gel methods exhibiting enhanced photocatalytic activity. Appl. Catal. B Environ. 89, 503–509.

Gao, X., Zhang, J., Zhang, L., 2002. Hollow sphere selenium nanoparticles: their in-vitro anti hydroxyl radical effect. Adv. Mater. 14, 290–293.

Geuenich, D., Hess, K., Köhler, F., Herges, R., 2005. Anisotropy of the induced current density (ACID), a general method to quantify and visualize electronic delocalization. Chem. Rev. 105, 3758–3772.

Graham, J.L., Loftin, K.A., Meyer, M.T., Ziegler, A.C., 2010. Cyanotoxin mixtures and taste-and-odor compounds in cyanobacterial blooms from the Midwestern United States. Environ. Sci. Technol. 44, 7361–7368.

Gritsenko, O., Ensing, B., Schipper, P., Baerends, E., 2000. Comparison of the accurate Kohn– Sham solution with the generalized gradient approximations (GGAs) for the SN_2 Reaction F-+ CH_3F→ FCH_3+ F-: a qualitative rule to predict success or failure of GGAs. J. Phys. Chem. A 104, 8558–8565.

Gupta, V., Ratha, S.K., Sood, A., Chaudhary, V., Prasanna, R., 2013. New insights into the biodiversity and applications of cyanobacteria (blue-green algae)-prospects and challenges. Algal Res. 2, 79–97.

Han, C., Pelaez, M., Likodimos, V., Kontos, A.G., Falaras, P., O'Shea, K., Dionysiou, D.D., 2011. Innovative visible light-activated sulfur doped TiO_2 films for water treatment. Appl. Catal. B Environ. 107, 77–87.

Han, F., Kambala, V.S.R., Srinivasan, M., Rajarathnam, D., Naidu, R., 2009. Tailored titanium dioxide photocatalysts for the degradation of organic dyes in wastewater treatment: a review. Appl. Catal. A-Gen. 359, 25–40.

Hoffmann, M.R., Martin, S.T., Choi, W., Bahnemann, D.W., 1995. Environmental applications of semiconductor photocatalysis. Chem. Rev. 95, 69–96.

Ji, W., Shen, Z., Fan, M., Su, P., Tang, Q., Zou, C., 2016. Adsorption mechanism of elemental mercury (Hg^0) on the surface of $MnCl_2$ (110) studied by Density Functional Theory. Chem. Eng. J. 283, 58–64.

Kandiel, T.A., Feldhoff, A., Robben, L., Dillert, R., Bahnemann, D.W., 2010. Tailored titanium dioxide nanomaterials: anatase nanoparticles and brookite nanorods as highly active photocatalysts. Chem. Mater. 22, 2050–2060.

Kapałka, A., Fóti, G., Comninellis, C., 2009. The importance of electrode material in environmental electrochemistry: formation and reactivity of free hydroxyl radicals on boron-doped diamond electrodes. Electrochim. Acta 54, 2018–2023.

Kohn, W., Becke, A.D., Parr, R.G., 1996. Density functional theory of electronic structure. J. Phys. Chem. 100, 12974–12980.

Kohtani, S., Tomohiro, M., Tokumura, K., Nakagaki, R., 2005. Photooxidation reactions of polycyclic aromatic hydrocarbons over pure and Ag-loaded $BiVO_4$ photocatalysts. Appl. Catal. B Environ. 58, 265–272.

Koppenol, W., Liebman, J.F., 1984. The oxidizing nature of the hydroxyl radical. A comparison with the ferryl ion (FeO^{2+}). J. Phys. Chem. 88, 99–101.

Lawton, L.A., Robertson, P.K., 1999. Physico-chemical treatment methods for the removal of microcystins (cyanobacterial hepatotoxins) from potable waters. Chem. Soc. Rev. 28, 217–224.

Lee, J., Walker, H.W., 2006. Effect of process variables and natural organic matter on removal of microcystin-LR by PAC-UF. Environ. Sci. Technol. 40, 7336–7342.

Li, Y., Ruan, Z., He, Y., Li, J., Li, K., Jiang, Y., Xu, X., Yuan, Y., Lin, K., 2018. In situfabrication of hierarchically porous g-C_3N_4 and understanding on its enhanced photocatalytic activity based on energy absorption. Appl. Catal. B Environ. 236, 64–75.

Liang, J., Li, Y., 2004. Synthesis and characterization of lead chromate uniform nanorods. J. Cryst. Growth 261, 577–580.

Liu, G., You, S., Huang, H., Ma, M., Ren, N., 2017a. A novel Z-scheme $BiPO_4$-Bi_2O_2(-OH)(NO_3) heterojunction structured hybrid for synergistic photocatalysis. Chemosphere 171, 702–709.

Liu, G., You, S., Ma, M., Huang, H., Ren, N., 2016. Removal of nitrate by photocatalytic denitrification using nonlinear optical material. Environ. Sci. Technol. 50, 11218–11225.

Liu, G., You, S., Tan, Y., Ren, N., 2017b. In situ photochemical activation of sulfate for enhanced degradation of organic pollutants in water. Environ. Sci. Technol. 51, 2339–2346.

Liu, G., You, S., Zhang, Y., Huang, H., Spanjers, H., 2019. Conjugated donor-acceptor (D-A) supramolecule catalyst for visible-light-driven photocatalytic removal of bromate in water. J. Colloid Interface Sci. 553, 666–673.

Liu, I., Lawton, L.A., Robertson, P.K., 2003. Mechanistic studies of the photocatalytic oxidation of microcystin-LR: an investigation of byproducts of the decomposition process. Environ. Sci. Technol. 37, 3214–3219.

Mei, Z., Shen, Z., Wang, W., Zhang, Y., 2007. Novel sorbents of non-metal-doped spinel Co_3O_4 for the removal of gas-phase elemental mercury. Environ. Sci. Technol. 42, 590–595.

Morales-Torres, S., Pastrana-Martínez, L.M., Figueiredo, J.L., Faria, J.L., Silva, A.M., 2012. Design of graphene-based TiO_2 photocatalysts-a review. Environ. Sci. Pollut. Res. 19, 3676–3687.

Paerl, H.W., Hall, N.S., Calandrino, E.S., 2011. Controlling harmful cyanobacterial blooms in a world experiencing anthropogenic and climatic-induced change. Sci. Total Environ. 409, 1739–1745.

Pan, C., Zhu, Y., 2010. New type of $BiPO_4$ oxy-acid salt photocatalyst with high photocatalytic activity on degradation of dye. Environ. Sci. Technol. 44, 5570–5574.

Pan, C., Zhu, Y., 2011. Size-controlled synthesis of $BiPO_4$ nanocrystals for enhanced photocatalytic performance. J. Mater. Chem. 21, 4235–4241.

Pelaez, M., Falaras, P., Likodimos, V., Kontos, A.G., Armah, A., O'shea, K., Dionysiou, D.D., 2010. Synthesis, structural characterization and evaluation of sol–gel-based NF-TiO_2 films with visible light-photoactivation for the removal of microcystin-LR. Appl. Catal. B Environ. 99, 378–387.

Rao, P., Hayon, E., 1974. Redox potentials of free radicals. I. Simple organic radicals. J. Am. Chem. Soc. 96, 1287–1294.

Schwarz, H., Dodson, R., 1984. Equilibrium between hydroxyl radicals and thallium (II) and the oxidation potential of hydroxyl (aq). J. Phys. Chem. 88, 3643–3647.

Shao, P., Duan, X., Xu, J., Tian, J., Shi, W., Gao, S., Xu, M., Cui, F., Wang, S., 2017. Heterogeneous activation of peroxymonosulfate by amorphous boron for degradation of bisphenol S. J. Hazard Mater. 322, 532–539.

Silva, C.G., Faria, J.L., 2010. Photocatalytic oxidation of benzene derivatives in aqueous suspensions: synergic effect induced by the introduction of carbon nanotubes in a TiO_2 matrix. Appl. Catal. B Environ. 101, 81–89.

Tang, J., Zou, Z., Ye, J., 2004. Effects of substituting Sr^{2+} and Ba^{2+} for Ca^{2+} on the structural properties and photocatalytic behaviors of $CaIn_2O_4$. Chem. Mater. 16, 1644–1649.

Turchi, C.S., Ollis, D.F., 1990. Photocatalytic degradation of organic water contaminants: mechanisms involving hydroxyl radical attack. J. Catal. 122, 178–192.

Wang, B., Xia, J., Mei, L., Wang, L., Zhang, Q., 2017. Highly efficient and rapid lead (II) scavenging by the natural Artemia cyst shell with unique three-dimensional porous structure and strong sorption affinity. ACS Sustain. Chem. Eng. 6, 1343–1351.

Wang, G., Chen, H., Li, Y., Kuang, A., Yuan, H., Wu, G., 2015. A hybrid density functional study on the visible light photocatalytic activity of (Mo, Cr)-N codoped $KNbO_3$. Phys. Chem. Chem. Phys. 17, 28743–28753.

Wang, W., Xu, C., Zhen, L., Shao, W., 2007. Single-crystalline $PbCrO_4$ nanorods: room temperature, surfactant free synthesis, characterization and optical property. J. Cryst. Growth 299, 86–93.

Yanfen, F., Yingping, H., Jing, Y., Pan, W., Genwei, C., 2011. Unique ability of BiOBr to decarboxylate d-Glu and d-MeAsp in the photocatalytic degradation of microcystin-LR in water. Environ. Sci. Technol. 45, 1593–1600.

You, S., Liu, B., Gao, Y., Wang, Y., Tang, C.Y., Huang, Y., Ren, N., 2016. Monolithic

porous Magnéli-phase Ti_4O_7 for electro-oxidation treatment of industrial wastewater. Electrochim. Acta 214, 326–335.
Zhang, G., Liu, G., Xu, Y., Yang, J., Li, Y., Sun, X., Chen, W., Su, C., 2018. $PbCrO_4$ yellow-pigment nanorods: an efficient and stable visible-light-active photocatalyst for O_2 evolution and photodegradation. Sci. China Mater. 61, 1033–1039.
Zhang, H., Zong, R., Zhao, J., Zhu, Y., 2008. Dramatic visible photocatalytic degradation performances due to synergetic effect of TiO_2 with PANI. Environ. Sci. Technol. 42, 3803–3807.
Zhang, Q., Yang, Q., Phanlavong, P., Li, Y., Wang, Z., Jiao, T., Peng, Q., 2017. Highly efficient lead (II) sequestration using size-controllable polydopamine microspheres with superior application capability and rapid capture. ACS Sustain. Chem. Eng. 5, 4161–4170.
Zhou, B., Zhao, X., Liu, H., Qu, J., Huang, C., 2010. Visible-light sensitive cobalt-doped BiVO4 (Co-BiVO4) photocatalytic composites for the degradation of methylene blue dye in dilute aqueous solutions. Appl. Catal. B Environ. 99, 214–221.